analytical chemistry

pubs.acs.org/ac Article

Absolute Cross Sections of Liquids from Broadband Stimulated Raman Scattering with Femtosecond and Picosecond Pulses

Kristen H. Burns, Prasenjit Srivastava, and Christopher G. Elles*

Cite This: *Anal. Chem.* 2020, 92, 10686−10692 Read Online

ABSTRACT: Broadband stimulated Raman scattering (SRS) is often observed in applications that use nonlinear spectroscopy to probe the composition or dynamics of complex systems. Whether the SRS response is measured intentionally or unintentionally, as a background signal, the relative scattering intensities provide a quantitative measure of the population profile of target molecules. Solvent scattering is a valuable internal reference for determining absolute concentrations in these applications, but accurate cross sections have been reported for only a limited number of transitions in select solvents and were measured using spontaneous Raman scattering with narrowband continuous wave or nanosecond light sources. This work reports the measurement and analysis of absolute Raman scattering cross sections spanning the frequency range of 500−4000 cm^{-1} for cyclohexane, DMSO, acetonitrile, methanol, water, benzene, and toluene using broadband SRS with femtosecond and picosecond Raman pump pulses at 488 nm. Varying the duration of the Raman pump pulses from ∼80 fs to >1 ps confirms that the cross sections are independent of the spectral bandwidth across the range of ∼250 to <20 cm^{-1}. The cross sections and depolarization ratios measured using broadband SRS agree with the limited number of previously reported values, after accounting for overlapping transitions in the lower-resolution femtosecond and picosecond spectra. The SRS cross sections reported here can be used with confidence as internal reference standards for a wide range of applications, including nonlinear spectroscopy and coherent microscopy measurements using ultrafast lasers.

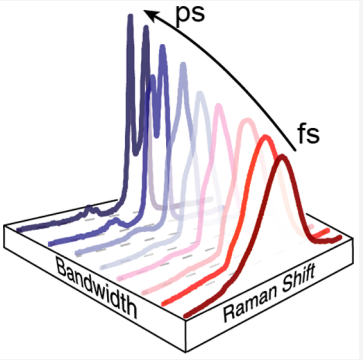

Coherent spectroscopy and microscopy techniques based on SERS, CARS, FSRS, two-photon absorption and fluorescence, and other methods are now widely used in measuring chemical dynamics,[1−4] probing the properties of inhomogeneous materials[5−8] and imaging biological systems.[9−13] Absolute cross sections are important for quantitative analysis of these measurements, particularly in cases where several components are present and contribute to the coherent scattering or absorption signal.[14−19] In most cases, accurate cross sections of target compounds are not directly available from a measurement but may be inferred based on the relative amplitude compared with the background signal from a solvent or other internal standard.[19−23] Given the relatively strong Raman response of many liquids,[24−26] stimulated Raman scattering (SRS) bands of a solvent provide a convenient reference for calibrating the intensity of a coherent signal. In this context, it is critical to know the absolute Raman scattering cross sections for specific vibrational bands of common solvents as well as the dependence of the scattering signal on the properties of the incident light.

Absolute Raman scattering cross sections have been reported for several liquids, but those measurements are limited to only one or two select vibrations of a molecule and were measured using spontaneous Raman scattering with narrowband continuous wave (cw) or nanosecond lasers.[21,22,27−30] In contrast, most coherent spectroscopies take advantage of the high peak intensity of femtosecond or picosecond laser pulses, which limits the spectral resolution due to the broader bandwidth inherent to short pulses. In order to provide a better reference for emerging coherent spectroscopy and microscopy applications, we measured broadband SRS cross sections for several common solvents using both femtosecond- and picosecond-duration Raman pump pulses. While the pulse duration affects the frequency resolution of the Raman spectrum, we show that accurate cross sections can be measured independently of the pulse width and that the measured cross sections are in excellent agreement with the handful of values available from spontaneous Raman scattering with higher frequency resolutions.

Specifically, we measure the differential Raman scattering cross sections of cyclohexane, dimethyl sulfoxide (DMSO), acetonitrile, methanol, water, benzene, and toluene using femto- and picosecond Raman pump pulses at 488 nm. In order to confirm that the cross sections are independent of the

Received: April 25, 2020
Accepted: June 29, 2020
Published: June 29, 2020

https://dx.doi.org/10.1021/acs.analchem.0c01785
Anal. Chem. 2020, 92, 10686−10692

pump pulse duration, we compare the differential Raman cross sections while varying the spectral bandwidth of the Raman pulses from 250 cm^{-1} to <20 cm^{-1}, corresponding to the typical range of bandwidths used in coherent spectroscopies. In addition to the transitions that were reported previously, we also report new Raman cross sections for several key vibrational bands in each of the seven solvents, including frequency-integrated cross sections covering the full range of C−H stretching vibrations measured using both femtosecond and picosecond pulses. We compare the full range of experimental SRS cross sections with theoretical values obtained from DFT calculations. The broad range of transitions that we report provides valuable quantitative information for a wide range of applications using nonlinear spectroscopy.

METHODS

We report the absolute stimulated Raman scattering cross sections for seven solvents, each with >99.9% purity. The organic solvents were used as received and without further purification, including cyclohexane (Fisher, certified ACS), dimethyl sulfoxide (Fisher, certified ACS), acetonitrile (Fisher, certified ACS), methanol (Fisher, HPLC grade), benzene (Sigma-Aldrich, HPLC grade), and toluene (Fisher, certified ACS). The water was deionized using an ion-exchange column.

Our broadband SRS measurements use the output of an amplified Ti:sapphire laser (Coherent, Legend Elite HP) that produces 35 fs pulses at a 1 kHz repetition rate. The fundamental is split into separate beams for generating the Raman pump and white-light probe pulses. We use an optical parametric amplifier (OPA) with two additional stages of second harmonic generation (SHG) to generate the Raman pump pulses at 488 nm, and we focus a small portion of the 800 nm fundamental into a circularly translating CaF_2 substrate to produce the broadband probe pulses via white-light continuum generation. Circular translation (rather than rotation) of the substrate maintains the alignment of the crystal axis and therefore preserves the vertical polarization of the probe light.

The pump pulses initially have <80 fs duration and >250 cm^{-1} bandwidth. Passing through a 4*f* spectral filter consisting of a grating, a cylindrical lens (f = 200 mm), and an adjustable slit reduces the bandwidth of the pump pulses to anywhere from ∼100 cm^{-1} when the slit is fully open (5 mm) to <20 cm^{-1} for a slit width of 0.15 mm. The spectral bandwidth for the 0.15 mm slit width is comparable to what we achieved previously using a 25 mm BBO crystal for the second stage of SHG, along with the 4*f* spectral filter.[31] Spectral compression using the longer BBO crystal results in higher transmission through the spectral filter but does not improve the frequency resolution (see Figure S1). Regardless of the bandwidth, we use a variable neutral density filter to attenuate the energy of the pump pulses to 0.40 ± 0.02 μJ at the sample.

The vertically polarized pump and probe beams overlap with a crossing angle of 4° in a 1 mm quartz cuvette containing the liquid sample. After the sample, the probe beam passes through a 750 nm short-pass filter and into a 1/8 m imaging spectrograph with an 1800 line/mm grating that disperses the light onto a 2068-pixel linear CCD array (Hamamatsu). The transmitted probe light is measured at 1 kHz, with the Raman pump being modulated at 500 Hz for active background subtraction. We use a delay stage to scan across the full interaction between the pump and probe pulses, averaging 3000 laser pulses per time delay for 3 consecutive scans. The result is a two-dimensional transient absorption spectrum, $A(\tau, \omega)$, that reveals the instantaneous Raman response as a function of the pump−probe delay and probe frequency, as shown in Figure S2. Using a pump pulse that is not resonant with any transitions in the sample ensures that there is no residual transient absorption signal when the pump and probe pulses do not overlap in time.

Integrating over the time delay between the pump and probe pulses at each probe frequency removes any contribution from dispersive interactions, such as cross-phase modulation,[32] and gives the full Raman response as a frequency-dependent SRS spectrum, $A(\omega)$. The amplitude $A(\omega)$ is proportional to the differential Raman scattering cross section, $\left(\frac{\partial^2\sigma}{\partial\Omega\,\partial\omega}\right)$, at probe frequency ω[33−35]

$$A(\omega) = \frac{1}{\ln 10}\cdot\frac{E_p LN}{\hbar\omega_p}\cdot\frac{16\pi^3 c^2}{n^2\omega^2}\cdot f_{xy}\cdot\left(\frac{\partial^2\sigma}{\partial\Omega\,\partial\omega}\right) \quad (1)$$

where E_p is the energy of the incident Raman pump pulse, L is the path length of the sample, N is the number density of the liquid, n is the index of refraction, ω_p is the Raman pump frequency, and f_{xy} represents the intensity-weighted spatial overlap of the pump and probe beams passing through the sample. The overlap factor, f_{xy}, assumes collinear pump and probe beams with Gaussian spatial profiles.[36] We measure the profile of each beam in both x and y dimensions at the position of the sample using the knife-edge technique (see Figure S3). Fitting each profile to an error function gives the $1/e^2$ half-widths, w_{pu} and w_{pr}, from which we obtain the overlap factor

$$f_{xy} = \frac{2}{\pi w_x w_y} \quad (2)$$

where $w_{x,y} = \sqrt{{w_{pu}}^2 + {w_{pr}}^2}$ are the half-widths in the x and y dimensions from a convolution of the two-dimensional Gaussian pump and probe beams. The pump−probe overlap is the primary source of uncertainty in determining absolute cross sections from SRS measurements, as we discuss below. Table S1 gives the number density and index of refraction that we use for each solvent.

The differential Raman scattering cross section, $\left(\frac{\partial^2\sigma}{\partial\Omega\,\partial\omega}\right)$, represents scattering into solid angle Ω, at frequency ω. The Raman scattering cross section is an intrinsic property of a material, and is the same for both spontaneous and stimulated Raman scattering.[2,24,35,37] We report the cross sections for individual Raman bands, $\left(\frac{\partial\sigma}{\partial\Omega}\right)$, by integrating over a frequency range that encompasses the full band. For overlapping transitions, we label the band according to the mode with the largest contribution. In the case of the C−H stretching vibrations, we report only the full integrated intensity of all Raman-active modes in the range ∼2800−3200 cm^{-1}.

We obtain theoretical Raman scattering cross sections from B3LYP/aug-cc-pVDZ calculations[38] using the GAUSSIAN software package.[39] The calculations give unpolarized Raman activities, S_n, in $Å^4$ amu^{-1}, from which we calculate the differential Raman scattering cross sections, $\left(\frac{d\sigma}{d\Omega}\right)_{unp}$, in cm^2 sr^{-1} $molecule^{-1}$.[40] In order to match our experimental conditions, we use depolarization ratios from the DFT

https://dx.doi.org/10.1021/acs.analchem.0c01785
Anal. Chem. 2020, 92, 10686−10692

calculations, ρ_s, to convert the unpolarized Raman cross sections to the values for parallel polarized light.[25]

$$\left(\frac{\partial\sigma}{\partial\Omega}\right)_{\parallel} = (1+\rho_s)^{-1}\cdot\left(\frac{\partial\sigma}{\partial\Omega}\right)_{\mathrm{unp}} \quad (3)$$

We restrict the geometry of each molecule in the calculations to retain the highest-symmetry point group.

RESULTS AND DISCUSSION

The SRS spectra for cyclohexane, DMSO, and acetonitrile are presented in Figure 1. The figure compares the spectra

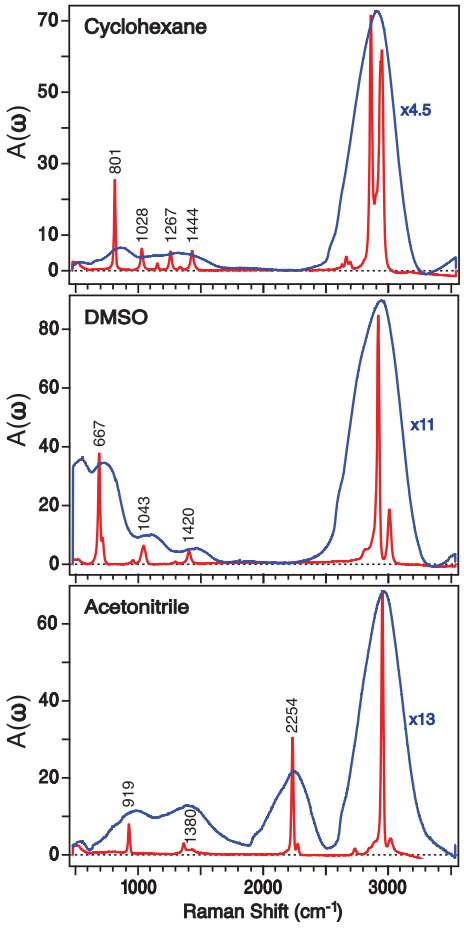

Figure 1. SRS spectra of cyclohexane, DMSO, and acetonitrile measured with 488 nm Raman pump pulses. In order to facilitate a comparison with the picosecond spectra (red lines), the intensities of the spectrally broadened femtosecond spectra (blue lines) are scaled by the indicated amounts.

obtained using both pico- and femtosecond Raman pump pulses. The spectra measured using the narrower bandwidth picosecond pump pulses have well-resolved transitions, whereas the femtosecond pump pulses give spectra that are much broader due to the larger bandwidth of the pulse. The strongest feature in each spectrum is the collection of C−H stretching vibrations near 3000 cm^{-1}; however, we also resolve lower-frequency vibrations depending on the structure of the molecule.

Similarly, Figure 2 shows the SRS spectra for methanol and water, where the probe range is shifted in comparison with the other solvents in order to show the full range of the O−H

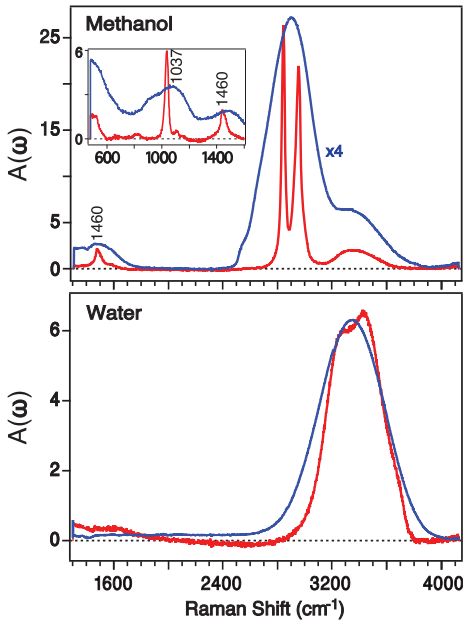

Figure 2. SRS spectra of methanol and water measured with 488 nm Raman pump pulses. In order to facilitate the comparison with the picosecond spectra (red lines), the intensities of the spectrally broadened femtosecond spectra (blue lines) are scaled by the indicated amounts. The inset shows the lower-frequency bands of methanol.

stretching vibration. The hydroxyl stretch is broad in both the picosecond and femtosecond spectra of each solvent due to hydrogen bonding.[28] For methanol, the O−H stretching band centered near 3400 cm^{-1} partially overlaps the C−H stretching modes in the femtosecond spectrum due to the broader bandwidth of the femtosecond pump pulses. In order to account for the overlapping intensity in the femtosecond spectrum, we determine the frequency-integrated cross sections of the C−H and O−H bands using a deconvolution with two Gaussian functions (Figure S4). The spectrum of water includes only the broad O−H stretching vibrations, for which we observe a distinctive double-peaked structure in the picosecond spectrum that matches previously reported spectra.[28] The structure is absent from the femtosecond spectrum of water due to the lower frequency resolution.

The SRS spectra for benzene and toluene are presented in Figure 3. The measurement in these solvents is complicated by overlapping two-photon absorption (2PA) bands at this combination of Raman pump and probe wavelengths.[34] The 2PA bands contribute to the time-integrated signal, $A(\omega)$, and result in additional features that are broader than the Raman transitions. The 2PA bands are more evident in the lower-resolution spectra, where we have expanded the scaling to compensate for the broadening and shortening of the Raman bands. However, the intensity and bandwidth of the 2PA signal is similar in both the high- and low-resolution spectra when viewed on the same scale (Figure S5) because the 2PA bands remain broad even at the higher resolution. In principle, the contributions from SRS and 2PA could be separated by changing the Raman pump wavelength, because the two signals shift in opposite directions in the probe spectrum. However, given the lower intensity and broader line widths of the 2PA features, we neglect the minor contribution to the Raman band integrals when calculating the cross sections.

https://dx.doi.org/10.1021/acs.analchem.0c01785
Anal. Chem. 2020, 92, 10686−10692

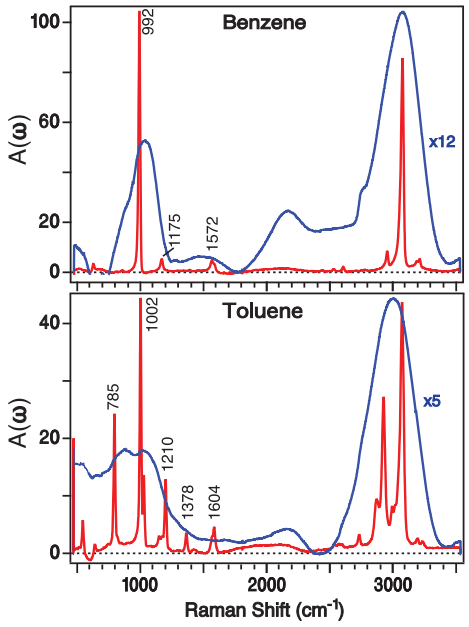

Figure 3. SRS spectra of benzene and toluene measured with 488 nm Raman pump pulses. In order to facilitate the comparison with the picosecond spectra (red lines), the intensities of the spectrally broadened femtosecond spectra (blue lines) are scaled by the indicated amounts.

The absolute Raman scattering cross sections for select bands in the spectrum of each solvent are summarized in Table 1. The table includes values that we obtain using both femtosecond and picosecond Raman pump pulses. The values for each band are in good agreement, within 20% on average, confirming that the integrated Raman cross sections are independent of the temporal pulse width and therefore the frequency resolution. The small discrepancies between the cross sections that we measure with femtosecond and picosecond pump pulses are likely a result of variations in the pump−probe overlap (f_{xy}) between the measurements and possibly also due to small contributions from baseline artifacts in the femtosecond spectra due to cross-phase modulation.

Table 1 also compares our Raman cross sections with values that were previously reported in the literature.[21,22,28−30] Absolute Raman scattering cross sections have been reported for only a limited number of vibrational bands of each solvent, and we are not aware of any previously reported values for DMSO at 488 nm. All of the previously reported values were measured using spontaneous Raman scattering at a collection angle of 90°. In general, our SRS cross sections are within ±20% of the literature values, which is a typical value of the uncertainty for absolute Raman measurements.[19,21] While our measurements are sensitive to the overlap between the pump and probe beams, spontaneous Raman measurements require precise knowledge of both the incident beam profile and collection conditions for the Raman scattering signal and often rely on comparisons with a photometric standard.[24] In any case, absolute cross sections typically have ∼20% or larger uncertainty, as is reflected in the variation between values reported by different authors.

The polarization dependence of the Raman cross sections complicates the comparison between values from different measurements. The literature values in Table 1 were measured with either parallel or unpolarized detection with respect to the incident light,[21,22,27−30] but we only report SRS cross sections measured with parallel polarization. Although depolarization ratios have been reported for all of the solvents in Table 1,[19,41−44] it can be difficult to compare the polarization dependence for measurements with different frequency resolutions, especially in cases where there are overlapping bands.[21,27] This issue is particularly acute for the lower-resolution spectra measured with femtosecond (and picosecond) pulses, where there are often several transitions underlying a single band. For example, the C−H stretching band of benzene consists of two closely spaced transitions that are only partially resolved even in higher-resolution spectra due to the natural line widths.[41]

We measure the polarization dependence of the benzene C−H stretching band in the SRS spectrum by rotating the polarization of the picosecond pump pulses using a zero-order wave plate. Integrating over the full Raman band at each polarization (Figure S6) gives a depolarization ratio of $\rho = A_{\perp}/A_{\parallel} = 0.312 \pm 0.013$ (2σ). This value is in good agreement with the average value of 0.32 from the individual depolarization ratios of the 3045 and 3062 cm^{-1} bands that were reported previously at a higher resolution.[41] The comparison is complicated by the overlapping bands and requires a weighted average of the two transitions, which is not straightforward to obtain from tabulated values in most cases. For the comparison with the experimental depolarization ratio, we obtain a value of 0.347 from DFT calculations (see below) by considering all of the transitions in the region of the C−H stretching modes. The discrepancy compared with the experimental values is due, at least in part, to the contributions from two weak shoulders in the experimental spectrum due to combination or overtone modes that are not present in our (harmonic) calculations. These complications highlight the difficulty in determining the polarization dependence for Raman cross sections in the femtosecond and picosecond spectra based on older measurements, providing additional motivation for new broadband SRS measurements.

For a comparison with the experimental values, Table 1 shows the calculated Raman cross sections from B3LYP/aug-cc-pVDZ for all of the solvents. The calculated values are converted from unpolarized Raman activities, S_n, to parallel-polarized Raman cross sections to match the experimental conditions (eq 3). A full list of values for the calculated vibrational frequencies, Raman activities, parallel and perpendicular cross sections, and depolarization ratios for each solvent are available in Table S2. The Raman cross sections, calculated for gas-phase molecules with a static incident frequency, are an average of ∼2.5 times smaller than the experimental values. The discrepancy is not surprising, because cross sections are known to be 2−4 times larger for liquids compared with isolated molecules, due to local field effects.[21,45,46] Pre-resonance enhancement is also likely to increase the experimental cross sections slightly, even for 488 nm excitation.[47] Nevertheless, the intensities within each spectrum are relatively insensitive to solvation in most cases,[38] allowing us to use the gas-phase calculations for comparison with the relative amplitudes and polarization dependence of our experimental spectra.

A key experimental parameter in our measurements is the duration of the Raman pump pulses, ranging from ∼80 fs to >1 ps. Raman scattering cross sections are an intrinsic property of the liquid, and the integrated intensity of a given Raman band should be independent of the pulse duration, and therefore

https://dx.doi.org/10.1021/acs.analchem.0c01785
Anal. Chem. 2020, 92, 10686−10692

Table 1. Differential Raman Scattering Cross Sections at 488 nm

		$\left(\frac{d\sigma}{d\Omega}\right)$ (10^{-30} cm^2 sr^{-1} molecule^{-1})			
solvent	band	ps pump[a]	fs pump[a]	literature	calculated[b]
cyclohexane	801 cm^{-1}	5.14		9.06[e], 11.3[f]	2.61
	1028 cm^{-1}	2.12		5.37[e]	0.78
	1267 cm^{-1}	1.64		4.61[e]	0.74
	1444 cm^{-1}	2.14		6.17[e]	0.88
	C−H[c]	47.70	60.06	75.2[e]	20.10
DMSO	667 cm^{-1}	8.22			6.22
	1043 cm^{-1}	2.02			0.66
	1420 cm^{-1}	1.42			0.57
	C−H[c]	22.14	23.74		8.03
acetonitrile	919 cm^{-1}	0.78		1.11[e]	0.48
	1380 cm^{-1}	1.14			0.57
	2254 cm^{-1}	2.84	2.10	3.71[e]	1.79
	C−H[c]	7.70	8.12	8.2[e]	4.62
methanol	1037 cm^{-1}	0.80		1.5[e], 2.5[f], 1.3[g]	0.49
	1460 cm^{-1}	0.46			0.32
	C−H[c]	7.20	8.50[d]	10.79[e], 5.7[g]	4.47
	O−H	1.84	2.04[d]	4.06[e]	0.76
water	O−H	3.52	4.42	8.2[h]	1.31
benzene	992 cm^{-1}	18.88	11.52	32.5[i], 36.5[j]	7.25
	1175 cm^{-1}	2.12			0.47
	1572 cm^{-1}	2.14			0.75
	C−H[c]	29.10	27.72	32.9[e], 57.1[i]	8.86
toluene	785 cm^{-1}	5.80			2.00
	1002 cm^{-1}	12.08		18.3[i]	3.93
	1210 cm^{-1}	4.40			0.96
	1378 cm^{-1}	0.90			0.45
	1604 cm^{-1}	1.68			0.84
	C−H[c]	37.94	38.14		13.41

[a]Estimated 2σ uncertainties are ±15% of the value. [b]B3LYP/aug-cc-pVDZ with parallel polarization. [c]Sum of all bands in the C−H stretching region. [d]From Gaussian deconvolution of C−H and O−H bands. [e]Ref 21, unpolarized. [f]Ref 27, unpolarized. [g]Ref 22, unpolarized. [h]Ref 28, unpolarized. [i]Ref 29, parallel. [j]Ref 30, unpolarized.

spectral resolution, provided all other experimental parameters remain constant (eq 1). To illustrate this point, Figure 4 shows the variation of the SRS spectrum in the C−H stretching region of cyclohexane (2400−3400 cm^{-1}) as we vary the spectral bandwidth of the Raman pump pulses. Closing the slit in the spectral filter narrows the bandwidth and increases the pulse duration, resulting in a higher frequency resolution and a better resolved Raman spectrum. Importantly, we attenuate the pump pulse energy to be the same for each measurement, regardless of the bandwidth.

The increasing spectral resolution with the pulse duration is evident in Figure 4a, where the spectrum of cyclohexane evolves from a single broad band encompassing all of the C−H stretching modes to a collection of bands comprising two, well-resolved peaks with an additional underlying structure due to the C−H stretching vibrations. The higher-resolution measurements also resolve a collection of weaker Raman bands near 2650 cm^{-1} due to overtones of the ring deformation modes.[48] Figure 4b shows the frequency-integrated SRS signal, A, for the full range of the C−H bands as a function of the spectral bandwidth of the Raman pump pulses. The inverse of the pulse duration provides an indirect measure of the spectral bandwidth due to the inverse relationship between the time and frequency. The pump pulse duration is easy to determine from the temporal profile of the Raman bands in the 2D spectrum, $A(\tau, \omega)$, as shown in Figure S8.[31]

The integrated SRS signals in Figure 4b are the same within the 10−15% uncertainty of the individual measurements, confirming that the measured cross section is independent of the bandwidth (or duration) of the pump pulse. The value for the uncertainty was determined based on our best estimate of the uncertainty in the spatial overlap of the pump and probe beams (f_{xy}), which is the primary source of the uncertainty in our measurement. Importantly, this is not the uncertainty from any single determination of the overlap using the knife-edge technique but rather our estimate (at 95% confidence) of the uncertainty for the method itself based on the variation across many independent measurements. Although we assume that both pump and probe beams have Gaussian spatial profiles, the variation of the pump beam leads to subtle differences in the measured signal strength. Filamentation in the white-light continuum generation process typically produces a very regular and Gaussian beam profile, but the mode of the pump beam generated in the OPA and two subsequent stages of the SHG is often distorted and may include "hot spots" that are difficult to characterize. Tuning the slit width in the spectral filter further distorts the beam profile, leading to variation in the weighted pump−probe overlap. These differences in the pump beam profile between measurements are too subtle to distinguish using the knife-edge technique and therefore are not properly accounted for in the weighted overlap factor, f_{xy}.

https://dx.doi.org/10.1021/acs.analchem.0c01785
Anal. Chem. 2020, 92, 10686−10692

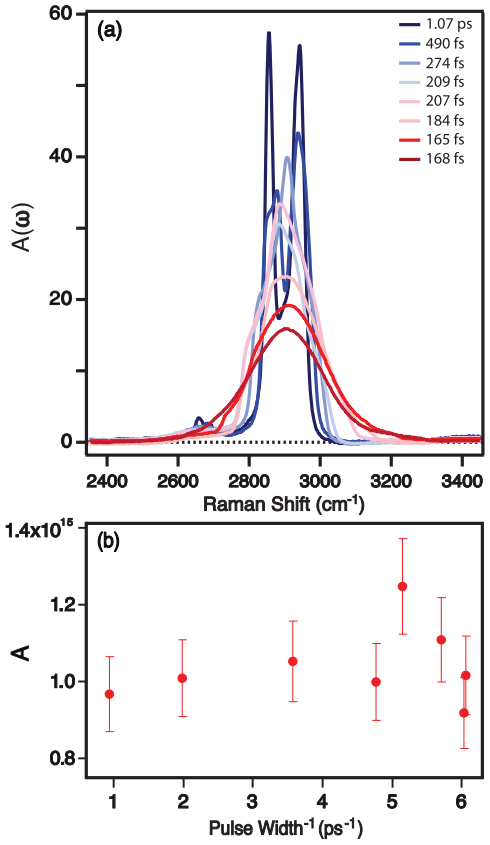

Figure 4. (a) Stimulated Raman spectrum of the C−H stretching region of cyclohexane for several different Raman pump pulse widths. (b) Frequency-integrated SRS signal in the range 2400−3400 cm^{-1}.

The variation of the beam profiles, and therefore of the pump−probe overlap, determines the overall uncertainty in the absolute Raman cross sections from our SRS measurements. We offer two examples to illustrate this variation, which is typical of any absolute Raman cross section measurement. On the basis of 24 independent measurements of the C−H stretching modes of cyclohexane (including two different experimental configurations), we estimate the uncertainty to be ±15% (2σ), giving a Raman cross section of $56 \pm 8 \times 10^{-30}$ cm^2 sr^{-1} $molecule^{-1}$. We find a similar uncertainty based on 16 independent measurements of the C−H stretching modes of benzene, for which we obtain a cross section of $26 \pm 4 \times 10^{-30}$ cm^2 sr^{-1} $molecule^{-1}$. These absolute cross sections for parallel polarization are slightly smaller than the unpolarized values previously reported in the literature, which are the sum of parallel and perpendicular polarization. However, our reported cross sections include small contributions from additional weak transitions that are not resolved in the lower-resolution femtosecond measurements in order to allow a direct comparison between the values measured with different pulse widths.

CONCLUSIONS

We measured and analyzed differential Raman scattering cross sections for seven common solvents using broadband SRS with picosecond and femtosecond pump pulses at 488 nm. A key result of this work is that the Raman cross sections measured using SRS are independent of the pulse width and are in good agreement with previously published values from spontaneous Raman scattering after accounting for overlapping transitions in the lower-resolution femtosecond (and picosecond) spectra. We also discuss the polarization dependence of the SRS bands with respect to the frequency resolution and the role of overlapping transitions. The solvent Raman bands provide a useful metric to determine the *in situ* polarization purity for any pump−probe or nonlinear spectroscopy measurement, but this approach requires careful consideration of the overlapping bands in the spectra measured with femtosecond and picosecond pump pulses compared with tabulated values from higher-resolution measurements. The broadband measurements reveal absolute cross sections for all Raman-active transitions in the range of 500−4000 cm^{-1}, allowing us to report accurate cross sections for several modes where they have not been reported previously. The wide range of accurate cross sections provides a useful reference for using Raman scattering as an internal standard. The internal standard technique has been widely used for measuring absolute cross sections from spontaneous Raman scattering, and the stimulated Raman values reported here will be especially valuable for applications in coherent spectroscopy and microscopy.

ASSOCIATED CONTENT

Supporting Information

The Supporting Information is available free of charge at https://pubs.acs.org/doi/10.1021/acs.analchem.0c01785.

Representative SRS spectra, solvent parameters, beam profiles, deconvolution of C−H and O−H bands of methanol, 2PA bands of benzene and toluene, polarization dependence of benzene C−H stretching bands, broadening of SRS spectra, temporal profiles of Raman response, calculated Raman spectra, optimized geometries, and frequencies for all seven solvents (PDF)

AUTHOR INFORMATION

Corresponding Author

Christopher G. Elles − *Department of Chemistry, University of Kansas, Lawrence, Kansas 66045, United States;* orcid.org/0000-0002-1408-8360; Email: elles@ku.edu

Authors

Kristen H. Burns − *Department of Chemistry, University of Kansas, Lawrence, Kansas 66045, United States*

Prasenjit Srivastava − *Department of Chemistry, University of Kansas, Lawrence, Kansas 66045, United States*

Complete contact information is available at: https://pubs.acs.org/10.1021/acs.analchem.0c01785

Notes

The authors declare no competing financial interest.

ACKNOWLEDGMENTS

This material is based upon work supported by the National Science Foundation under Grant Number CHE-1905334. The authors wish to thank Marco Caricato and Matthew S. Barclay for many helpful discussions and David A. Stierwalt for contributions at an early stage.

REFERENCES

(1) Frontiera, R. R.; Henry, A. I.; Gruenke, N. L.; Van Duyne, R. P. *J. Phys. Chem. Lett.* **2011**, *2*, 1199−1203.

(2) McAnally, M. O.; Phelan, B. T.; Young, R. M.; Wasielewski, M. R.; Schatz, G. C.; Van Duyne, R. P. *Anal. Chem.* **2017**, *89*, 6931−6935.
(3) Xiong, H.; Qian, N.; Miao, Y.; Zhao, Z.; Min, W. *J. Phys. Chem. Lett.* **2019**, *10*, 3563−3570.
(4) Yang, J. M.; Jin, L.; Pan, Z. Q.; Zhou, Y.; Liu, H. L.; Ji, L. N.; Xia, X. H.; Wang, K. *Anal. Chem.* **2019**, *91*, 6275−6280.
(5) Marin, B. C.; Hsu, S.-W.; Chen, L.; Lo, A.; Zwissler, D. W.; Liu, Z.; Tao, A. R. *ACS Photonics* **2016**, *3*, 526−531.
(6) Shutov, A. D.; Yi, Z.; Wang, J.; Sinyukov, A. M.; He, Z.; Tang, C.; Chen, J.; Ocola, E. J.; Laane, J.; Sokolov, A. V.; Voronine, D. V.; Scully, M. O. *ACS Photonics* **2018**, *5*, 4960−4968.
(7) Ling, J.; Miao, X.; Sun, Y.; Feng, Y.; Zhang, L.; Sun, Z.; Ji, M. *ACS Nano* **2019**, *13*, 14033−14040.
(8) Miao, K.; Wei, L. *ACS Cent. Sci.* **2020**, *6*, 478.
(9) Silva, W. R.; Keller, E. L.; Frontiera, R. R. *Anal. Chem.* **2014**, *86*, 7782−7787.
(10) Kim, D.; Choi, D. S.; Kwon, J.; Shim, S. H.; Rhee, H.; Cho, M. *J. Phys. Chem. Lett.* **2017**, *8*, 6118−6123.
(11) Shi, L.; Xiong, H.; Shen, Y.; Long, R.; Wei, L.; Min, W. *J. Phys. Chem. B* **2018**, *122*, 9218−9224.
(12) Hill, A. H.; Fu, D. *Anal. Chem.* **2019**, *91*, 9333−9342.
(13) Lenzi, E.; Jimenez De Aberasturi, D.; Liz-Marzán, L. M. *ACS Sensors* **2019**, *4*, 1126−1137.
(14) Larkin, P. J.; Gustafson, W. G.; Asher, S. A. *J. Chem. Phys.* **1991**, *94*, 5324−5330.
(15) Ouyang, S. L.; Sun, C. L.; Zhou, M.; Li, Z. L.; Men, Z. W.; Li, D. F.; Li, Z. W.; Gao, S. Q.; Lu, G. H. *J. Raman Spectrosc.* **2010**, *41*, 1650−1654.
(16) Mafra, D. L.; Kong, J.; Sato, K.; Saito, R.; Dresselhaus, M. S.; Araujo, P. T. *Nano Lett.* **2012**, *12*, 2883−2887.
(17) Buchanan, L. E.; McAnally, M. O.; Gruenke, N. L.; Schatz, G. C.; Van Duyne, R. P. *J. Phys. Chem. Lett.* **2017**, *8*, 3328−3333.
(18) Acosta-Maeda, T. E.; Misra, A. K.; Porter, J. N.; Bates, D. E.; Sharma, S. K. *Appl. Spectrosc.* **2017**, *71*, 1025−1038.
(19) Bray, A.; Chapman, R.; Plakhotnik, T. *Appl. Opt.* **2013**, *52*, 2503−2510.
(20) Shim, S.; Stuart, C. M.; Mathies, R. A. *ChemPhysChem* **2008**, *9*, 697−699.
(21) Nestor, J. R.; Lippincott, E. R. *J. Raman Spectrosc.* **1973**, *1*, 305−318.
(22) Griffiths, J. E. *J. Chem. Phys.* **1974**, *60*, 2556−2557.
(23) Krivenkov, V.; Samokhvalov, P.; Dyagileva, D.; Karaulov, A.; Nabiev, I. *ACS Photonics* **2020**, *7*, 831−836.
(24) Prince, R. C.; Frontiera, R. R.; Potma, E. O. *Chem. Rev.* **2017**, *117*, 5070−5094.
(25) Long, D. A. *The Raman Effect:a unified treatment of the theory of Raman scattering by molecules*; Wiley: New York, NY, 2002; p 597.
(26) McCreery, R. L. *Raman Spectroscopy for Chemical Analysis*; Wiley, 2000; p 420.
(27) Colles, M. J.; Griffiths, J. E. *J. Chem. Phys.* **1972**, *56*, 3384−3391.
(28) Marshall, B. R.; Smith, R. C. *Appl. Opt.* **1990**, *29*, 71.
(29) Kato, Y.; Takuma, H. *J. Opt. Soc. Am.* **1971**, *61*, 347−350.
(30) Schomacker, K. T.; Delaney, J. K.; Champion, P. M. *J. Chem. Phys.* **1986**, *85*, 4240−4247.
(31) Pontecorvo, E.; Ferrante, C.; Elles, C. G.; Scopigno, T. *Opt. Express* **2013**, *21*, 6866−6872.
(32) Kovalenko, S. A.; Dobryakov, A. L.; Ruthmann, J.; Ernsting, N. P. *Phys. Rev. A: At., Mol., Opt. Phys.* **1999**, *59*, 2369−2384.
(33) Isobe, K.; Kawano, H.; Suda, A.; Kumagai, A.; Miyawaki, A.; Midorikawa, K. *Biomed. Opt. Express* **2013**, *4*, 1548.
(34) Houk, A. L.; Givens, R. S.; Elles, C. G. *J. Phys. Chem. B* **2016**, *120*, 3178−3186.
(35) Lee, D.; Albrecht, A. C. *A unified view of Raman, resonance Raman and fluorescence spectroscopy (and their analogues in two-photon absorption)*; Clark, R. J. H., Hester, R. E., Eds.; Wiley, 1985; Vol. *12*, Chapter 4, pp 179−213.
(36) Elles, C. G.; Rivera, C. A.; Zhang, Y.; Pieniazek, P. A.; Bradforth, S. E. *J. Chem. Phys.* **2009**, *130*, 084501.
(37) McCamant, D. W.; Kukura, P.; Mathies, R. A. *Appl. Spectrosc.* **2003**, *57*, 1317−1323.
(38) Barclay, M. S.; Elles, C. G.; Caricato, M. *J. Chem. Theory Comput.* **2020**, *16*, 612−620.
(39) Frisch, M. J.; Trucks, G. W.; Schlegel, H. B.; Scuseria, G. E.; Robb, M. A.; Cheeseman, J. R.; Montgomery, J. A., Jr.; Vreven, T.; Kudin, K. N.; Burant, J. C.; Millam, J. M.; Iyengar, S. S.; Tomasi, J.; Barone, V.; Mennucci, B.; Cossi, M.; Scalmani, G.; Rega, N.; Petersson, G. A.; Nakatsuji, H.; Hada, M.; Ehara, M.; Toyota, K.; Fukuda, R.; Hasegawa, J.; Ishida, M.; Nakajima, T.; Honda, Y.; Kitao, O.; Nakai, H.; Klene, M.; Li, X.; Knox, J. E.; Hratchian, H. P.; Cross, J. B.; Bakken, V.; Adamo, C.; Jaramillo, J.; Gomperts, R.; Stratmann, R. E.; Yazyev, O.; Austin, A. J.; Cammi, R.; Pomelli, C.; Ochterski, J. W.; Ayala, P. Y.; Morokuma, K.; Voth, G. A.; Salvador, P.; Dannenberg, J. J.; Zakrzewski, V. G.; Dapprich, S.; Daniels, A. D.; Strain, M. C.; Farkas, O.; Malick, D. K.; Rabuck, A. D.; Raghavachari, K.; Foresman, J. B.; Ortiz, J. V.; Cui, Q.; Baboul, A. G.; Clifford, S.; Cioslowski, J.; Stefanov, B. B.; Liu, G.; Liashenko, A.; Piskorz, P.; Komaromi, I.; Martin, R. L.; Fox, D. J.; Keith, T.; Al-Laham, M. A.; Peng, C. Y.; Nanayakkara, A.; Challacombe, M.; Gill, P. M. W.; Johnson, B.; Chen, W.; Wong, M. W.; Gonzalez, C.; Pople, J. A. *Gaussian 03*, Revision D.01; Gaussian, 2004.
(40) Neugebauer, J.; Reiher, M.; Kind, C.; Hess, B. A. *J. Comput. Chem.* **2002**, *23*, 895−910.
(41) Proffitt, W.; Porto, S. P. S. *J. Opt. Soc. Am.* **1973**, *63*, 77.
(42) Kiefer, J. *Anal. Chem.* **2017**, *89*, 5725−5728.
(43) Kaye, W.; McDaniel, J. B. *Appl. Opt.* **1974**, *13*, 1934.
(44) Bogaard, M. P.; Buckingham, A. D.; Pierens, R. K.; White, A. H. *J. Chem. Soc., Faraday Trans. 1* **1978**, *74*, 3008−3015.
(45) Asher, S. A.; Johnson, C. R. *J. Phys. Chem.* **1985**, *89*, 1375−1379.
(46) Fernández-Sánchez, J. M.; Montero, S. *J. Chem. Phys.* **1989**, *90*, 2909−2914.
(47) Dudik, J. M.; Johnson, C. R.; Asher, S. A. *J. Chem. Phys.* **1985**, *82*, 1732−1740.
(48) Skobel tsyn, D. *Optical Studies in Liquids and Solids*, 39th ed.; 1969; p 265.

https://dx.doi.org/10.1021/acs.analchem.0c01785
Anal. Chem. 2020, 92, 10686−10692